Attenuation of Voltage Distortion Effects on a Three-Phase Grid-Connected Converter

Mauro Boi, Andrea Floris, Alessandro Serpi, Alfonso Damiano
Dipartimento di Ingegneria Elettrica ed Elettronica
Universitá degli Studi di Cagliari
Cagliari,Italy

***Abstract*—The paper reports the power quality improvement of a grid-connected three-phase voltage source converter (VSC) aimed at interfacing electrochemical energy storage to the power system. Two control algorithms have been synthesised and experimentally validated, considering an LCL-filter VSC that implements a current feedback control on a synchronous reference frame. The comparison between a proportional-integral (PI) controller with a hybrid one, characterised by the joining of PI and resonant (R) controllers, specifically designed for reducing the effects of fifth and seventh voltage harmonics, has been performed. The PI-R controller outcomes show a significant improvement concerning PI one regarding the total harmonic distortion of the injected converter current for output power values lower than the 30% of rated one. This solution permits the extension of the lower power limit for which the current total harmonic distortion is lower than 5%, till to 18%. Therefore, the hybrid PI-R controller results are suitable for those applications, such as the energy storage system, requiring power quality in an ample range of working operative conditions.**

***Index Terms*—Grid connected converter, PI controller, resonant controller, energy storage systems.**

I. Introduction

Energy storage systems (ESSs) will play a crucial role in the de-carbonization process of power systems because they will support the integration of the expected massive exploitation of Renewable Energy Sources (RES). ESSs assure power balancing, power quality and reliability at the same time. Moreover, due to their versatility, power scalability, efficiency and dynamic characteristics, ESS can provide ancillary services, contributing to achieving the power flexibility requested in awaited RES-based power systems [1].

The stationary ESSs are generally composed of three subsystems: the electrochemical battery, the battery management system (BMS) and the power conversion one. The latter permits bidirectional management of power flows between the electrochemical battery and the grid. Typically, the power conversion topology is characterized by a cascade connection of DC/DC and DC/AC converters. The DC/DC converter manages the DC power flow between the battery and DC/AC converter, preserving compliance with the battery constraints. The DC/AC converter performs the bidirectional power flow between DC and AC sides according to specific standards, assuring high efficiency and dynamic performances [2]. Furthermore, the DC/AC converter has to guarantee the compliance with specific standards for proper integration into the power system. Regarding power quality, the IEEE 1547-2018 specifies the limit of each harmonic order and the total rated-current distortion (TRD) that should not exceed 5% for the first fifty-odd harmonic currents [3]. However, the TRD refers to the converter's rated current and does not consider the power quality performance under variable power conditions typical of RES and ESS.

The current harmonics generated by the voltage source converter (VSC) are mainly due to power electronics' dead times and voltage distortions at the point of common coupling (PCC). Nevertheless, the dead time can be compensated by predicting algorithms, whereas the grid voltage distortion directly impacts the VSC determining the injection of corresponding harmonic currents [4] [5].

The latter issue is particularly critical in weak networks because it depends on the local configuration of the distribution network and loads. Therefore, the voltage distortion cannot be standardized regarding harmonic contents. In addition, the injected current harmonic components, associated with corresponding voltage ones, sustain and enforce harmonic distortion, further impairing the power quality. For this reason, developing VSC robust to harmonic voltage pollution represents a crucial topic for assuring the sustainable integration of RES and ESS in the power system [6].

The phenomena mentioned above are also influenced by control schemes implemented on VSCs [7]. Specifically, the use of a phase-locked loop (PLL), required for synchronizing the VSC, is directly affected by voltage distortions [8], [9]. Moreover, the grid voltage is generally used as a feed-forward in the current control loop to improve the dynamic and robustness performances and reduce the control efforts, introducing, in such manner, the grid-voltage distortions into the control loop [2]. This approach is typically implemented in VSC's current control schemes independently of the reference frame adopted. Specifically, current control algorithms implemented in the stationary reference frame (SRF) resort to a proportional-resonant (PR) controller, which requires PLL to

This research was funded by Regione Autonoma della Sardegna-Accordo di Collaborazione tra Enti Pubblici-Art. 15 della Legge 7 Agosto 1990 No. 241 for the development of the project "Solare Termodinamico per lo sviluppo di una rete per la Gestione Intelligente dell'Energia Elettrica e Termica"—Grant No.: Cup I58I18000350002.

generate the current set-points on $\alpha - \beta$ axes [10]. The three-phase grid-connected VSCs implementing LCL filter perform the current control in the synchronous reference frame $(d-q)$ resorting to a proportional-integral (PI) controller supported by grid voltage feed-forward [11]. Also, in this case, the PLL assumes the fundamental role of implementing the Park's transformations. Furthermore, particular attention has to be spent on setting the PI parameters in accordance with LCL filter ones to avoid that feedback control causing resonance, which leads to system instability [12], [13].

In scientific literature, different solutions have been proposed to mitigate the effects of voltage distortion on VSC. Specifically, the implementation of proportional resonant plus multi-resonant (PR-MR) controllers allows the selective attenuation of specific harmonic components resorting to multi-low-order harmonic resonant banks tuned for performing a selective compensation [14]. A practical application of this concept has recently been proposed for mitigating the VSC odd harmonic currents in the range between 5^{th} to 13^{th}. Particularly, adding the fundamental controller in the stationary reference frame of four PR multi-resonant controllers characterized by a specific resonance and damping frequency has allowed the reduction of injected current THD until the achievement of 1.1% [15]. Another approach is the proper management of voltage feed-forward or the use of higher-order PLL algorithms. Implementing full-feed-forward functions of grid voltages for a three-phase LCL-type grid-connected inverter permits the reduction of grid current harmonics and unbalance caused by grid voltages [16].

In this context, the proposed research activity aims to mitigate the power intermittency of the High Concentrator Photovoltaic power plant (HCPV). Specifically, the proper use of a local weather forecasting algorithm combined with real-time control allows the definition of balancing power profiles provided by a Sodium Metal Halide battery (SMHB) ESS [17]. The proposed research activity aims to develop a high-quality VSC for interfacing an ESS based on SMHB able to provide the power service required for this specific application in the presence of distorted grid voltage arising in weak networks, typical conditions occurring in sites where these plants are installed. The SMHB-ESS and its grid-connected three-phase SiC-based power converter have been specifically designed referring to a specific case study [11], [18]. The performance evaluation highlighted that the minimum power value, for which the THD of output VSC current is less than 5%, has to be greater than 30% of rated power. Therefore, further improvements have been investigated to make the proposed configuration more robust to the grid voltage distortions.

II. Case Study

The case study is an ESS used to support a microgrid (MG) supplied by an HCPV power plant. Specifically, the investigation has been developed on a test bench that reproduces scaled conditions occurring in the Ottana MG [17]. The test bench is installed at the Technology Park of Sardinia (TePoS) and is composed of an HCPV power plant, reported in Fig.1,

Fig. 1. Case study: HCPV power plant.

TABLE I
Technical Specifications of the HCPV Plant

Rated power @$850W/m^2$	P_{mpp}	6.2	kW
Short-circuit current	I_{sc}	8.5	A
Open circuit voltage	V_{oc}	800	V
MPPT current @$850W/m^2$	I_{mpp}	7.6	A
Collecting Area	A_{cpv}	30	m^2
Overall efficiency	η_{cpv}	25	%

and electronic loads that reproduce the scaled evolution of electricity demand in TePoS [19]. The HCPV has a rated AC power of 6.2 kW (@ DNI value of 850W/m^2), and the overall rated efficiency is 25%. The collecting system comprises 90 modules fixed on a dual-axis solar tracker with a positioning accuracy of 0.1° degree. The main parameters are reported in Table I.

A. Sodium Metal Halide Battery

The energy storage device installed for supporting the HCPV power plant is an SMHB. Due to its features, this electrochemical battery is among the most suitable technology for stationary energy storage applications [20]. The installed SMHB is FIAMM SoNick battery model ST523, available on the market. It has 240 cells connected in series enclosed in a metallic container thermally isolated. The FIAMM SoNick ST523 is equipped with an electric heater for keeping the battery temperature within its operative range. The main operating data of the SMHB are reported in Table II.

TABLE II
SMHB characteristics of FIAMM SoNick ST523

Rated power	P_{bat}	7.8	kW
Rated voltage	V_{bat}	620	V
Energy Capacity	E_{bat}	23.5	kWh
Calendar life @80 **of DOD**		15	y
Cycle-life @80 **of DOD**		4500	$cycles$
Rated Temperature	T_{bat}	270	$°C$

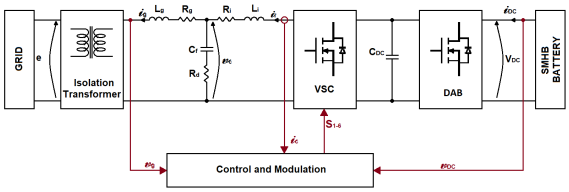

Fig. 2. Schematic of proposed ESS configuration.

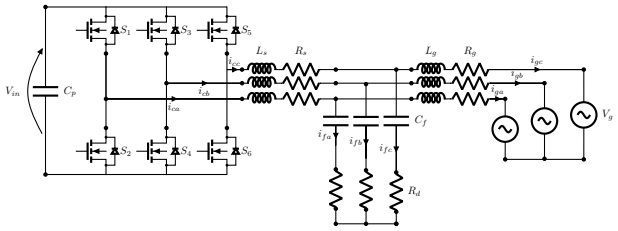

Fig. 3. Schematic of SiC based inverter.

III. Grid-connected inverter

The interconnection of SMHB on the MG requires a grid-connected converter. The schematic configuration of the proposed ESS is reported in Fig.2. A three-phase VSC implementing LCL filter has been designed employing high-performance components such as Silicon Carbide (SiC) mosfet.

An insulation transformer of 8kVA has been interposed between the filter and VSC. The DC bus of the power converter is connected to SMHB, employing a DC/DC converter [18]. The schematic representation of the three-phase grid-connected inverter is reported in Fig.3. The converter design refers to rated quantities of the case study reported in Table III. Precisely, the SiC-based inverter is carried out by resorting to the parallel connection of three half-bridges whose main characteristics are in Table IV. The half-bridge converter is equipped with two SiC power mosfets C2M0080120D whose main characteristics are in Table V. The half-bridge board implements all necessary circuits for proper and safe operation [11]. The total DC bus capacitance C_{DC}^{tot} of the three-phase inverter is equal to 780 μF.

A. LCL filter

The VSC switching frequency harmonics are limited, resorting to passive filters. In this case, a wye LCL filter has been designed referring to specifications reported in Table III [11]. The evaluation of the LCL parameters has been defined by resorting to an iterative procedure aimed at respecting all the constraints in terms of: maximum power factor; the minimum voltage drop on the total value of inductance; the resonant frequency of LCL filter, and attenuation of current ripple at the switching frequency respect to the value expected on converter side [13]. The LCL filter parameters are reported in TableVI. Intending to avoid resonance phenomena, the filter design has been developed such that the filter resonant frequency f_{res} is equal to 1610 Hz according to the criterion that suggests $10f_g < f_{res} < f_{sw}/2$, where f_g and f_{sw} are the grid and the VSC' switching frequencies, respectively [13].

TABLE III
Design Specifications

Rated power	P_r	8	kVA
Rated grid voltage	V_g	400	V_{RMS}
Rated current	I_r	11.5	A_{RMS}
Ratel grid frequency	f_g	50	Hz
Rated switching frequency	f_{sw}	20	kHz
DC-link voltage	V_{DC}	700	V

TABLE IV
Half-Bridge module rating

DC Bus voltage	V_{DC}	800	V
Maximum continuous current	I_{DC}^{max}	24	A_{RMS}
Maximum pulsed current	I_{DC}^{pulsed}	80	A
reference switching frequency	f_{sw}	20	kHz
DC side bus capacitance	C_{DC}	260	μF

TABLE V
SiC Mosfet C2M0080120D Maximum Ratings

Drain-Source Voltage	V_{ds}	1200	V
Continuous Drain Current	I_D^{SiC}	24	A
Power Dissipation	P_D^{SiC}	192	W
reference switching frequency	f_{sw}	20	kHz
Drain-Source On-State Resistance	R_{ds}^{on}	128	$m\Omega$
Turn-On Switching Energy	E_{on}^{sw}	265	μJ
Turn-Off Switching Energy	E_{off}^{sw}	135	μJ

IV. VSC Current control

The VSC control strategy has been synthesised referring to the synchronous rotating frame, according to the model reported in (1). The control structure has been implemented as shown in Fig.4. In particular, the synchronous reference frame phase-locked loop (SRF-PLL) allows identifying instantaneous position θ of grid voltage space vector [21]. Implementing Clark and Park transformations allows the evaluation of currents $i_d\, i_q$ and voltages $v_d\, v_q$ on $d-q$ axes, synchronous with the rotating frame. The application of voltage feed-forward and the cancellation of current cross-coupling permit the

TABLE VI
LCL Filter Parameters

Insulation transformer inductance	L_t	$0,68$	mH
Grid side inductance	L_g	$2,2$	mH
Resistance of grid side inductance	R_g	65	$m\Omega$
Converter side inductance	L_i	$2,2$	mH
Resistance of converter side inductance	R_i	65	$m\Omega$
Capacitor - Wye connection	C_f	10	μF
Damping resistance	R_d	1	Ω

decoupling of current loops. In such a manner, the synthesis of PI regulator parameters can be performed according to linear control theory. Setting the current bandwidth at $150\,Hz$, the PI parameters k_p and k_i assume the values of 5 $[V/A]$ and 553 $[V/As]$, respectively. The simulation and experimental results have confirmed the achievement of design targets. However, the experimental investigation regarding the power quality of output currents and input voltages highlighted the presence of current total harmonic distortion less than 5% just for an output power greater than 30% of the rated one. This is mainly ascribed to grid voltage harmonic distortions [11]. In order to overcome this issue, the PI regulator has been integrated with Resonant Controller (RC). In particular, the harmonic analysis of grid voltage outlined that the fifth and the seventh components significantly contribute to VSC current distortion. Hence, considering that in the synchronous reference frame these two harmonics have the same absolute frequency (6 ω_g), using a single resonant controller on each current loop to mitigate the voltage effects produced by the fifth and seventh harmonics has been investigated [14]. Particularly, the resonant controller whose model is reported in (2) has been implemented as reported in Fig.4. The parameter K_i is the controller gain, ω_c is the resonant bandwidth and $6\,\omega_g$ is the resonance frequency. The Z-transformation of (2) performed through Backward-Euler allows the evaluation of the digital model of resonant controller reported in (3). The parameters of the digital controller have been evaluated by setting the K_i and ω_c at a value equal to one and imposing on the synchronous reference frame a resonance frequency of 300 Hz. [22]. The sampling period T_{sw} has been set to 50μs. Hence, resorting to (4-6) the digital controller parameters have been defined, achieving the values reported in Table VII.

$$\begin{aligned} v_d &= R\,i_d + L\,\frac{d\,i_d}{dt} + \omega_s\,L\,i_q + u_d; \\ v_q &= R\,i_q + L\,\frac{d\,i_q}{dt} - \omega_s\,L\,i_d + u_q; \end{aligned} \tag{1}$$

$$RC(s) = \frac{V(s)}{\Delta(s)} = \frac{K_i\,\omega_c\,s}{s^2 + 2\,\omega_c\,s + (6\,\omega_g)^2}. \tag{2}$$

$$RC(z) = \frac{b_0 + b_1\,z^{-1} + b_2\,z^{-2}}{a_0 + a_1\,z^{-1} + a_2\,z^{-2}}. \tag{3}$$

$$\begin{aligned} b_0 &= K_i\,\omega_c\,T_{sw}. \\ b_1 &= \Big[-K_i\,\omega_c\,e^{(-0.5\omega_c\,T_{sw})} \\ &\quad cos\left(T_{sw}\cdot\sqrt{(6\,\omega_g)^2 - 0.25\omega_c^2}\right) - C\Big]\,T_{sw} \\ b_2 &= 0. \end{aligned} \tag{4}$$

where C is a constant defined as

$$\begin{aligned} C = &\frac{0.5\,K_i\,\omega_c^2}{\sqrt{(6\,\omega_g)^2 - 0.25\omega_c^2}}\,e^{(-0.5\omega_c\,T_{sw})}. \\ &\cdot\ sin\left(T_{sw}\sqrt{(6\,\omega_g)^2 - 0.25\omega_c^2}\right) \end{aligned} \tag{5}$$

TABLE VII
PARAMETERS OF DIGITAL PR CONTROLLER

a_0	a_1	a_2	b_0	b_1	b_2
1	-1.99	0.99	$0.471\,10^{-3}$	$-0.469\,10^{-3}$	0

$$\begin{aligned} a_0 &= 1. \\ a_1 &= -\,2\,e^{(-0.5\omega_c\,T_{sw})}\,cos\left(T_{sw}\,\sqrt{(6\,\omega_g)^2 - 0.25\omega_c^2}\right) \\ a_2 &= e^{-\omega_c\,T_{sw}} \end{aligned} \tag{6}$$

V. SIMULATION AND EXPERIMENTAL RESULTS

The proposed grid-connected power converter, including the filter and the isolation transformer, has been simulated on the Plecs environment. In order to evaluate the performances of the control technique, the simulations have been developed employing the voltage measurements sampled on the TePoS' MG, characterised by a harmonic distortion typical of real system and reported in Fig.11. The aforementioned control algorithm characterised by joining of PI and resonant (R) controllers, has been implemented on Matlab/Simulink environment, employing as feedback the current data sampled on Plecs. The control system's output is the modulation signal of VSC used in co-simulation with Plecs to perform the management of power electronic devices according to space vector modulation. The simulation results confirm the achievement of design performances. Subsequently, the simulation results have been compared with the experimental one considering different operative conditions and implementing exactly the same code used during the simulations. The proposed control algorithms have been implemented on a rapid prototyping controller (B-Box RCP 3.0) employing Matlab/Simulink. The sampling frequency in the case under analysis has been set at $20kHz$, the same of simulations. Three isolated voltage sensors with a measurement bandwidth of 60 kHz, accuracy of 0,15 % and input range voltage of 800 V have been installed on PCC. Three insulated current measurement sensors (LAH 50-P) carry out the feedback signals for current loop control.

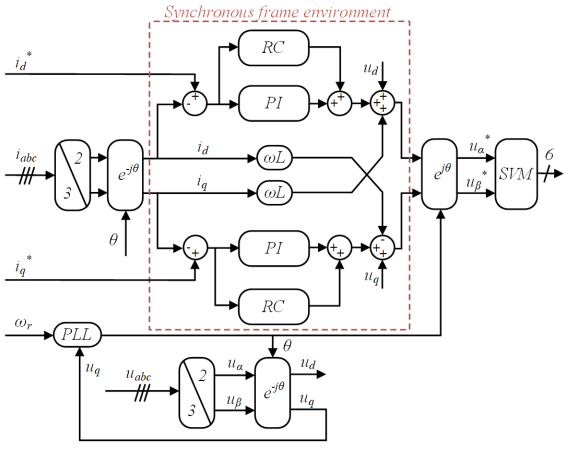

Fig. 4. Schematic of current control system of power converter.

The final version of the prototype under test is reported in Fig.5

The comparison between simulation and the experimental results has been performed considering the implementation of the proposed PI-R controller on the $d-q$ axes and the PI one. The performance evaluation has been developed for different current conditions. Specifically, in Fig.6 is reported the evolutions of the currents injected by the VSC on the power system when a set-point of 3 A and PI-R controllers are implemented. The comparison between the simulation and experimental results well match permitting the validation of the simulation model regarding the evaluation of steady state effects associate to voltage distortions on the VSC. The same test has been performed with the use of just the PI controller. The comparison between the simulation and experimental results is reported in Fig. 7. The same comparison has been developed for a different current set-point equal to 10 A. The results are reported in Fig.8 and Fig.9, respectively.

The evaluation of the current THD has been executed by employing WT 5000 power analyser. The results reported in Fig.10 compare the measured current THD v.s. VSC output power when the PI-R controller and the PI one are implemented on proposed VSC. A significant improvement is obtained by PI-R controller concerning the PI one in the range of power output between 0 and 0.4 p.u.. Specifically, a THD lower that 5% is achieved for a rated power of 18 % for which the PI regulator assume a value of 8%. A detailed analysis of current harmonic content is reported in Fig.11 that shows the strict correlation between the harmonic voltage content, in accordance with the scientific literature [23]. Moreover, this analysis highlights the effect in term of mitigation of the PI-R controller. Specifically, the effect of the PR halves the fifth and seventh harmonic components respect to the corresponding ones misused during the usage of PI regulator. The comparison of the efficiency evolution respect to the power does not show significant differences between the two analysed configurations.

VI. Conclusion

The present paper presents a comparison between a proportional-integral controller and a hybrid one, characterised by the joining of PI and resonant (R) controllers. The hybrid controller has been synthesised to mitigate the effects of voltage distortion, focusing specifically on the main harmonic components of a weak power system, i.e. fifth and seventh voltage harmonics. The proposed PI-R controller has been synthesised to extend the lower power limit for which the total harmonic distortion is lower than 5%. The proposed algorithm has been simulated and finally implemented on a prototype. The experimental results highlight improvements of the PI-R controller concerning the PI one in terms of

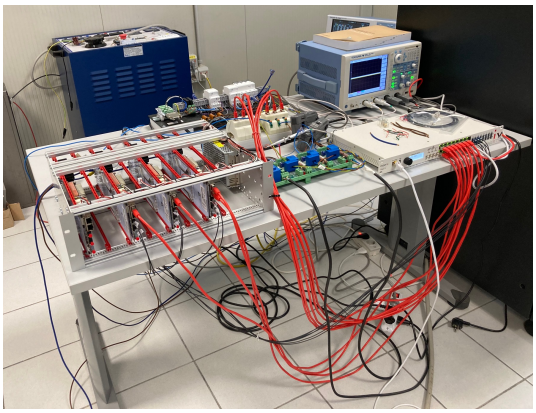

Fig. 5. Test bench of the three phase grid-connected VSC.

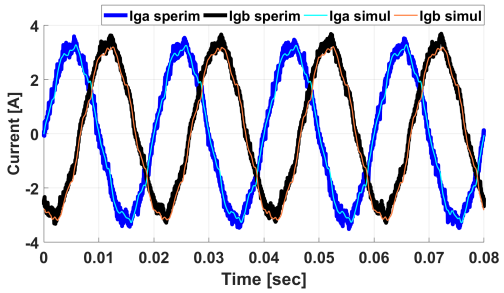

Fig. 6. Comparison between simulation and experiment results of i_α and i_β for a current set-point of 3 A with the implementation of PR controller.

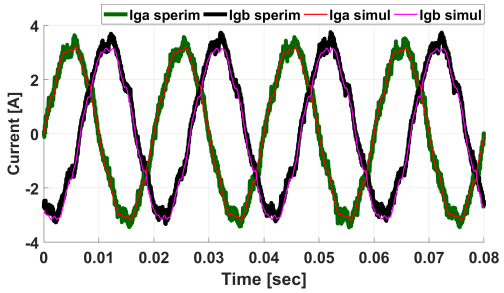

Fig. 7. Comparison between simulation and experiment results of i_α and i_β currents at 3 A without PR controller.

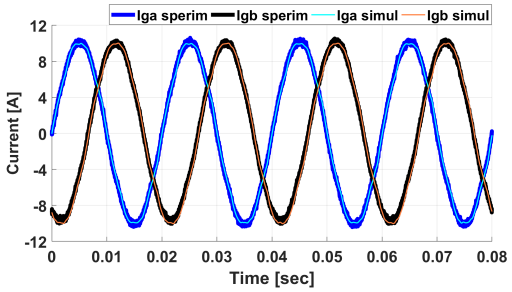

Fig. 8. Comparison between simulation and experiment results of i_α and i_β currents at 10 A with PR controller.

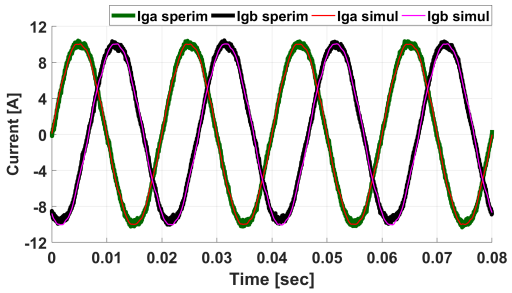

Fig. 9. Comparison between simulation and experiment results of i_α and i_β currents at 10 A without PR controller.

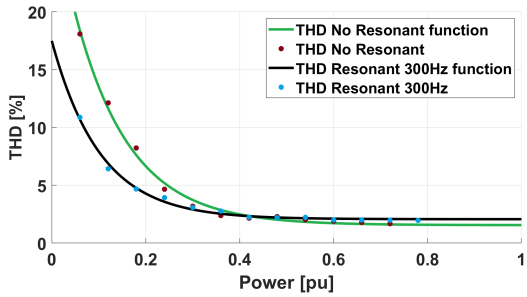

Fig. 10. Comparison between current THD v.s. output VSC power with (blue trace) and without (green trace) PR controller

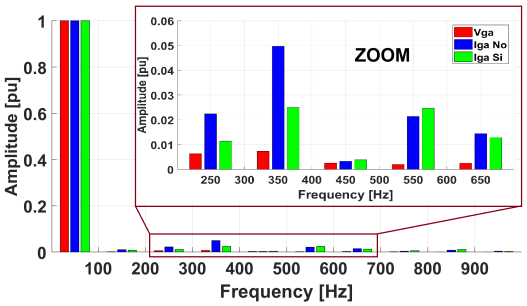

Fig. 11. Comparison between the normalized grid side current and voltage spectrum at 18% of rated power with (green bar) and without (blue bar) PR .

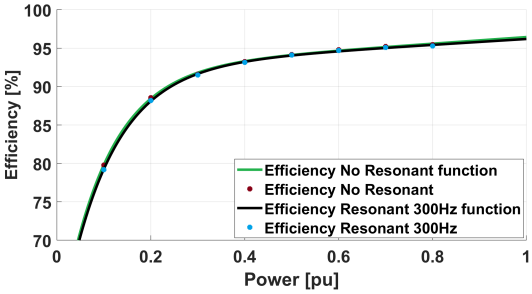

Fig. 12. Evaluation of power converter efficiency respect to output power with (green trace) and without (blue trace) PR.

extension of minimum power value with respect to the rated one for which the current total harmonic distortion is lower than 5%. Specifically, a minimum value of 18% of rated power has been achieved concerning a 25% obtainable implementing PI regulator. Power quality improvement does not impair efficiency performance. Therefore, the hybrid PI-R controller results are suitable for those applications, such as the energy storage system, requiring power quality in an ample range of working operative conditions.

REFERENCES

[1] A. Serpi, M. Porru, and A. Damiano, "An optimal power and energy management by hybrid energy storage systems in microgrids," *Energies*, vol. 10, pp. 1–21, Nov. 2017.

[2] J. Rocabert, A. Luna, F. Blaabjerg, and P. Rodríguez, "Control of power converters in ac microgrids," *IEEE Transactions on Power Electronics*, vol. 27, no. 11, pp. 4734–4749, 2012.

[3] "Ieee standard for interconnection and interoperability of distributed energy resources with associated electric power systems interfaces–amendment 1: To provide more flexibility for adoption of abnormal operating performance category iii," *IEEE Std 1547a-2020 (Amendment to IEEE Std 1547-2018)*, pp. 1–16, 2020.

[4] Y. Y. Yang, K. Zhou, H. Wang, and F. Blaabjerg, "Analysis and mitigation of dead-time harmonics in the single-phase full-bridge pwm converter with repetitive controllers," *IEEE Transactions on Industry Applications*, vol. 54, no. 5, p. 5343–5354, 2018.

[5] T. Abeyasekera, C. Johnson, D. Atkinson, and M. Armstrong, "Suppression of line voltage related distortion in current controlled grid connected inverters," *IEEE Transactions on Power Electronics*, vol. 20, no. 6, pp. 1393–1401, 2005.

[6] X. Liang and C. Andalib Bin-Karim, "Harmonics and mitigation techniques through advanced control in grid-connected renewable energy sources: A review," *IEEE Transactions on Industry Applications*, vol. 54, no. 4, pp. 3100–3111, 2018.

[7] M. Kazmierkowski and L. Malesani, "Current control techniques for three-phase voltage-source pwm converters: a survey," *IEEE Transactions on Industrial Electronics*, vol. 45, no. 5, pp. 691–703, 1998.

[8] F. Blaabjerg, R. Teodorescu, M. Liserre, and A. Timbus, "Overview of control and grid synchronization for distributed power generation systems," *IEEE Transactions on Industrial Electronics*, vol. 53, no. 5, pp. 1398–1409, 2006.

[9] J. Rocabert, A. Luna, F. Blaabjerg, and P. Rodríguez, "Control of power converters in ac microgrids," *IEEE Transactions on Power Electronics*, vol. 27, no. 11, pp. 4734–4749, 2012.

[10] D. G. Holmes, T. A. Lipo, B. P. Mcgrath, and W. Y. Kong, "Optimized design of stationary frame three phase ac current regulators," *IEEE Transactions on Power Electronics*, vol. 24, no. 11, p. 2417–2426, 2009.

[11] M. Boi and A. Damiano, "Evaluation of sic-based three phase power converter for microgrid applications," in *IECON 2022 – 48th Annual Conference of the IEEE Industrial Electronics Society*, 2022, pp. 1–7.

[12] J. Dannehl, C. Wessels, and F. W. Fuchs, "Limitations of voltage-oriented pi current control of grid-connected pwm rectifiers with *lcl* filters," *IEEE Transactions on Industrial Electronics*, vol. 56, no. 2, pp. 380–388, 2009.

[13] M. Liserre, F. Blaabjerg, and S. Hansen, "Design and control of an lcl-filter-based three-phase active rectifier," *IEEE Transactions on Industry Applications*, vol. 41, no. 5, pp. 1281–1291, 2005.

[14] M. Liserre, R. Teodorescu, and F. Blaabjerg, "Multiple harmonics control for three-phase grid converter systems with the use of pi-res current controller in a rotating frame," *IEEE Transactions on Power Electronics*, vol. 21, no. 3, pp. 836–841, 2006.

[15] A. A. Nazeri, C. Noeding, and P. Zacharias, "High-performance grid current feedback control for three-phase voltage-source converter with an lcl filter under distorted grid conditions," in *IECON 2022 – 48th Annual Conference of the IEEE Industrial Electronics Society*, 2022, pp. 1–8.

[16] W. Li, X. Ruan, D. Pan, and X. Wang, "Full-feedforward schemes of grid voltages for a three-phase *lcl*-type grid-connected inverter," *IEEE Transactions on Industrial Electronics*, vol. 60, no. 6, pp. 2237–2250, 2013.

[17] A. Salimbeni, M. Porru, L. Massidda, and A. Damiano, "A forecasting-based control algorithm for improving energy managment in high concentrator photovoltaic power plant integrated with energy storage systems," *Energies*, vol. 13, no. 18, 2020.

[18] M. Boi, A. Salimbeni, A. Damiano, L. P. Di Noia, and R. Rizzo, "A triple-port active bridge dc-dc converter for integration of energy storage systems in concentrator photovoltaic," in *2021 IEEE 15th International Conference on Compatibility, Power Electronics and Power Engineering (CPE-POWERENG)*, 2021, pp. 1–7.

[19] M. Gawronska, C. S. Piattaforma, S. Casula, A. Salimbeni, and A. Damiano, "A test bench for microgrids powered by concentrator photovoltaic systems," in *2017 6th International Conference on Clean Electrical Power (ICCEP)*, 2017, pp. 262–268.

[20] M. Boi, D. Battaglia, A. Salimbeni, and A. Damiano, "A novel electrical model for iron doped-sodium metal halide batteries," *IEEE Transactions on Industry Applications*, vol. 55, no. 6, pp. 6247–6255, 2019.

[21] S. Golestan, J. M. Guerrero, and J. C. Vasquez, "Three-phase plls: A review of recent advances," *IEEE Transactions on Power Electronics*, vol. 32, no. 3, pp. 1894–1907, 2017.

[22] T. D. C. Busarello, J. A. Pomilio, and M. G. Simoes, "Design procedure for a digital proportional-resonant current controller in a grid connected inverter," in *2018 IEEE 4th Southern Power Electronics Conference (SPEC)*, 2018, pp. 1–8.

[23] W. Li, X. Ruan, D. Pan, and X. Wang, "Full-feedforward schemes of grid voltages for a three-phase lcl type grid-connected inverter," *IEEE Transactions on Industrial Electronics*, vol. 60, no. 6, pp. 2237–2250, 2013.